

Study of structural, magnetic and magneto-transport properties of nanocrystalline $\text{La}_{2/3}\text{Ca}_{1/3}\text{MnO}_3$ manganite

A. GAUR^{*}, U. KR. GAUR^a, K. YADAV^a, G. D. VARMA^a

Department of Physics, National Institute of Technology, Kurukshetra-136116, India

^aDepartment of Physics, Indian Institute of Technology, Roorkee-247667, India

The nanocrystalline $\text{La}_{2/3}\text{Ca}_{1/3}\text{MnO}_3$ samples were prepared by sol-gel method and were sintered at different temperatures ranging from 600°C to 1000°C. It has been found that the magnetic and transport properties of the samples strongly depend on the sintering temperature. Decreasing the sintering temperature causes a substantial decrease in insulator-metal transition temperature (T_{IM}) and enhancement in resistivity. Reduction in magnetization and slight decrease in paramagnetic-ferromagnetic (PM-FM) transition temperatures (T_{c}) has been observed as the sintering temperature decreases. The MR at $T < T_{\text{c}}$ increases on decreasing the sintering temperature as well as on increasing the applied magnetic field. However, at/around T_{c} the intrinsic contribution of MR occurs which is more in the samples sintered at higher temperatures. These variations in MR are explained by enhanced spin polarized tunneling by assuming the increase of grain boundary contribution as the sintering temperature decreases.

Received May 31 2010; accepted July 14, 2010)

Keywords: Electrical transport, Nanocrystalline, Grain boundaries

1. Introduction

The discovery of colossal magnetoresistance (CMR) in mixed-valence manganese perovskites of the type $\text{La}_{1-x}\text{Ca}_x\text{MnO}_3$ has motivated a wide research on these compounds [1, 2]. The CMR properties of these compounds make them technologically important for applications in magnetoresistive devices. Earlier studies revealed that for $x \sim 1/3$, the maximum CMR is observed at the insulator-metal (IM) transition temperature (T_{IM}), usually accompanied by a simultaneous paramagnetic-ferromagnetic transition at the Curie temperature (T_{c}) [3]. Besides the CMR, growing attention is also being paid to another kind of magnetoresistance (MR), namely, the extrinsic or intergrain MR, found in polycrystalline manganites [4-8]. The extrinsic MR appears in the temperature range of $T < T_{\text{IM}}$ and increases with lowering the temperature from T_{IM} . Although the CMR near T_{c} is an intrinsic property of manganites and double exchange (DE) mechanism is the most prominent theory of explaining the major results of intrinsic CMR. While extrinsic MR is associated to grain boundaries or interfaces, which is important source of low-field magnetoresistance (LFMR) in polycrystalline samples. This LFMR or grain boundary MR is due to spin-polarized tunneling between neighbouring grains [4-5, 9] and is important for applications. Although the actual mechanism of LFMR response for polycrystalline manganite samples is still obscure but it is undoubted that the effect of grain boundaries plays key roles in the LFMR. As a consequence, the preparation of perovskite manganite via sol-gel has been a continuous interest [6, 10] because by this technique we can modify the grain boundaries on growing the nanosized particles. So, improved MR could be achieved for the nanosized perovskite manganite

samples prepared through sol-gel process. The sol gel process also has other potential advantages over other traditional processing techniques such as better homogeneities, low processing temperature and improved material properties [11]. Although, there are several reports [12-16] on the synthesis of nanophasic manganite by sol-gel based methods but none of them seems to have carried out systematic studies on the sintering temperature effect on magnetotransport properties of $\text{La}_{2/3}\text{Ca}_{1/3}\text{MnO}_3$ system.

In the present work, by a comparative study, we examine the influence of sintering temperature on a particular composition of Ca-doped system ($\text{La}_{2/3}\text{Ca}_{1/3}\text{MnO}_3$) prepared via sol-gel process. We observed that transport and magnetoresistance properties of this $\text{La}_{2/3}\text{Ca}_{1/3}\text{MnO}_3$ system strongly depend on the sintering temperature (T_{s}). The samples were sintered at different temperatures ranging from 600°C to 1000°C. Some salient features observed as we reduce the sintering temperature are (i) a decrease in magnetization and PM-FM transition temperature (T_{c}), (ii) an increase in the resistivity and suppression in I-M transition temperature (T_{MI}), (iii) enhancement in magnetoresistance especially at low temperatures which is attributed to a spin-polarized intergrain tunneling mechanism [17]. These observations are logically explained by assuming the increase of grain boundary contribution as the sintering temperature decreases [18-20].

2. Experimental details

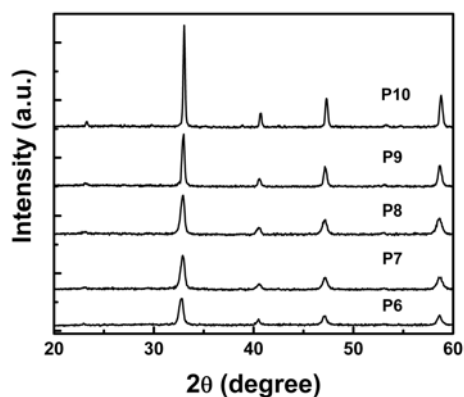
The nanocrystalline samples of $\text{La}_{0.67}\text{Ca}_{0.33}\text{MnO}_3$ (LCMO) were synthesized via sol-gel method. The required amounts of high purity nitrates of La, Ca and Mn

were dissolved in the double distilled water to form an aqueous solution. An equal amount of ethylene glycol was added to this solution with continuous stirring. This solution was then heated on a hot plate at temperature of ~80-100°C till a dry thick brown sol was formed. This was further decomposed in an oven at a temperature of 250°C to get the dry fluffy material. This obtained polymeric precursor was calcined at 350°C for 12 h. The resulting powder was separated into parts and pressed in the form of pellets and sintered for 10h at 600°C, 700°C, 800°C, 900°C and 1000°C. The samples sintered at 600°C, 700°C, 800°C, 900°C and 1000°C are referred to as P6, P7, P8, P9, and P10, respectively. The structural characterization was examined by using X-ray diffraction (Bruker AXS D-8 advance, CuK_α radiation) technique at room temperature and surface morphology was investigated by using a scanning electron microscope (SEM Model LEO 435-VP operating at 15 KV). Resistivity as a function of temperature was measured by a standard four-probe method by using Keithley instruments without or with magnetic fields (0-10 kOe). The DC magnetization measurements were done by using vibrating sample magnetometer (VSM Model 155, Princeton Applied Research).

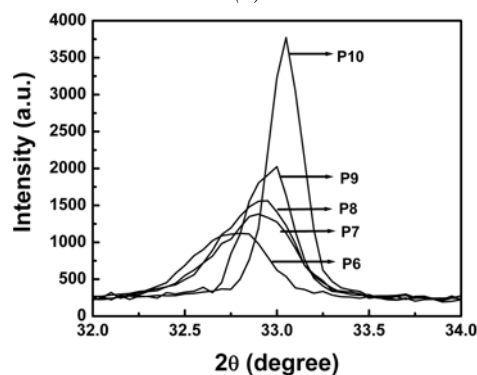
3. Results and discussion

The room temperature X-ray diffraction patterns of the studied samples are shown in Fig. 1(a). Results indicate that all the samples P6, P7, P8, P9 and P10 sintered at temperature of 600°C, 700°C, 800°C, 900°C and 1000°C, respectively are in pure single LCMO phase with no detectable secondary phase within the accuracy of measurement. The complete pure LCMO phase has been obtained at the temperature as low as 600°C.

The intensity of diffraction peaks for LCMO perovskite phase increases as the sintering temperature increases from 600°C to 1000°C indicating that the crystallinity of LCMO becomes better and particle size increases as sintering temperature increases. Fig. 1 (b) shows the (121) reflection (near $2\theta=33^\circ$) of P6, P7, P8, P9, and P10 samples.



(a)



(b)

Fig. 1. (a) X-ray diffraction patterns of the $\text{La}_{2/3}\text{Ca}_{1/3}\text{MnO}_3$ samples sintered at 600°C (P6), 700°C (P7), 800°C (P8), 900°C (P9) and 1000°C (P10); (b) Shows the comparison of most intense (121) peak for the $\text{La}_{2/3}\text{Ca}_{1/3}\text{MnO}_3$ samples sintered at different temperatures.

It is clear from the Fig. 1(b) that as sintering temperature increases, the intensity of the (121) reflection increases and there is a decrease in full width at half maximum (FWHM), hence the particle size increases. The shifting of (121) peak towards higher value of Bragg angle indicates that the lattice parameters decrease as the sintering temperature increases. The calculated lattice parameters (orthorhombic unit cell parameters a, b, c) and cell volume of unit cell ($V=abc$) are shown in Table 1.

Table 1. Variation of lattice parameters, cell volumes, particle size and grain size of $\text{La}_{2/3}\text{Ca}_{1/3}\text{MnO}_3$ samples with sintering temperature.

Sample name	Sintering temperature (°C)	Lattice parameters			Cell volume (Å^3)	Particle size (nm) (by XRD)	Grain size (nm) (by SEM)
		a (Å)	b(Å)	c(Å)			
P6	600	5.455	7.708	5.459	229.5353	~23	~32
P7	700	5.435	7.678	5.469	228.2209	~25	~54
P8	800	5.417	7.645	5.479	226.9016	~28	~72
P9	900	5.430	7.646	5.458	226.6040	~44	~145
P10	1000	5.416	7.626	5.464	225.6764	~67	~254

It is observed that the cell volume of the unit cell decreases as particle size increases. The average particle sizes of the samples are estimated from X-ray data using Scherrer's formula ($PS \sim K \lambda / \beta \cos \theta$ where $k \sim 0.89$ is the

shape factor, λ is wavelength of x-rays, β is the FWHM and θ is Bragg angle) [21]. The calculated average particle sizes are ~23nm, ~25nm, ~28nm, ~44nm and ~67nm for the samples sintered at 600°C, 700°C, 800°C, 900°C and

1000°C respectively. The representative SEM images of the samples P7, P8, P9, and P10 are shown in Fig. 2(a)-(d), respectively. SEM pictures reveal that grain size increases and porosity decreases as sintering temperature increases. It also can be seen from SEM pictures that the grain boundaries in sample (P7) are not clear and there is a long neck between two grains. With the increase of sintering temperature from sample (P7) to sample (P10), the size of grain becomes larger, the grain boundaries become obvious, grain connectivity improves and the necks among grains disappear. The average grain sizes measured from SEM micrographs are $\sim 54\text{nm}$, $\sim 72\text{nm}$, $\sim 145\text{nm}$ and $\sim 254\text{nm}$ for the samples P7, P8, P9, and P10, respectively. There is a variation between particle sizes obtained from the width of XRD peaks and the grain sizes obtained from SEM (see Table 1). Both particle size and grain size increase as the sintering temperature increases. However, it has been observed that there is a difference between particle size and grain size at all sintering temperature and is more pronounced at higher sintering temperature. This difference is due to the fact that grains are composed of several particles, which may introduce the internal stress or defects in the structure.

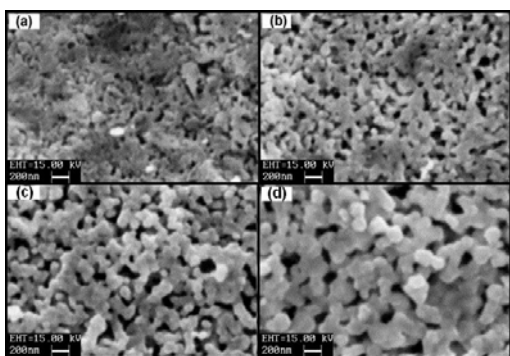


Fig. 2. Scanning electron micrographs of $\text{La}_{2/3}\text{Ca}_{1/3}\text{MnO}_3$ samples sintered at different temperatures (a) 700°C (P7), (b) 800°C (P8), (c) 900°C (P9) and (d) 1000°C (P10).

The magnetization curves of all the samples measured under 5kOe field in the temperature range (80-300K) are shown in Fig. 3.

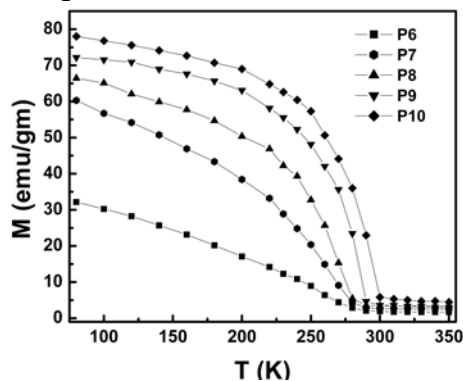


Fig. 3. Magnetization as a function of temperature measured at 5 kOe of $\text{La}_{2/3}\text{Ca}_{1/3}\text{MnO}_3$ samples.

All the samples show the PM-FM transition at a particular temperature (T_c). We observed a slight variation in T_c for the samples sintered at different temperatures. The transition temperatures determined from the peak in $dM/dT-T$ curves are found to be $\sim 258\text{K}$, $\sim 262\text{K}$, $\sim 269\text{K}$, $\sim 280\text{K}$ and $\sim 288\text{K}$ for samples P6, P7, P8, P9, and P10, respectively. Moreover, in our case, the magnetization decreases as the sintering temperature decreases. The value of magnetization (M) at 80K for the samples P6, P7, P8, P9 and P10 are 32.16emu/gm, 60.30emu/gm, 66.41emu/gm, 72.17emu/gm and 78.01emu/gm, respectively. The reduction in magnetization with decreasing the sintering temperature may be because of changing the lattice geometry as lattice parameters and cell volume change and formation of extra grain boundaries as particle size reduces, causes broken Mn-O-Mn bonds at the surface that hamper exchange interaction and resulting decrease in magnetization. This is general observation in case of nanoparticles of the manganite system as found by others [18, 22]. Zhang et al [23] also analyzed in detail the effect of the annealing on the magnetization of the samples with various x values in $\text{La}_{1-x}\text{Sr}_x\text{MnO}_3$ system. They found that at low doping ($x < 0.25$), the magnetization decreases with an increase in sintering temperature and for higher doping ($x > 0.25$), the magnetization increases with an increase in sintering temperature. So our results match with Zhang et al [23] results, i.e. for $x > 0.25$, magnetization decreases with decreasing the sintering temperature and grain boundaries play the role in reduction of magnetization. It has also been observed that as the sintering temperature decreases the width of transition broadens which suggests that at low sintering temperature grains are loosely connected and also are visible in the scanning electron micrograph shown in Fig. 2. The magnetization versus field ($M-H$) curve at 80K for the studied samples is displayed in Fig. 4.

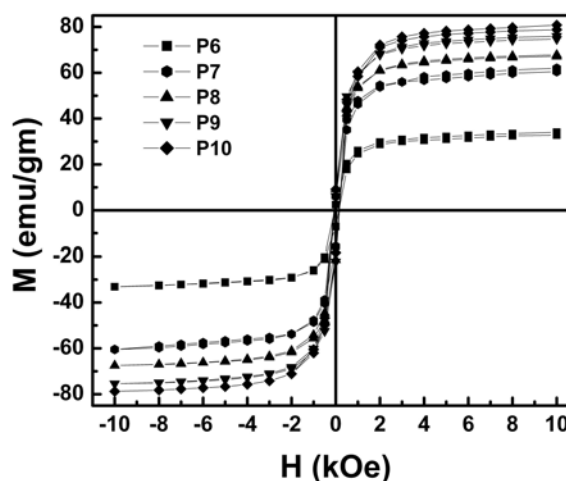


Fig. 4. Magnetization versus field ($M-H$) curves at 80K of $\text{La}_{2/3}\text{Ca}_{1/3}\text{MnO}_3$ samples.

$M-H$ curves also show that the magnetization of the samples decreases with decreasing the sintering temperature. This demonstrates that ferromagnetic order is

weakened and magnetic disorder increases on reducing the sintering temperature.

The temperature dependence resistivity measured in temperature range (80-300K) at zero field for the studied samples is shown in Fig. 5.

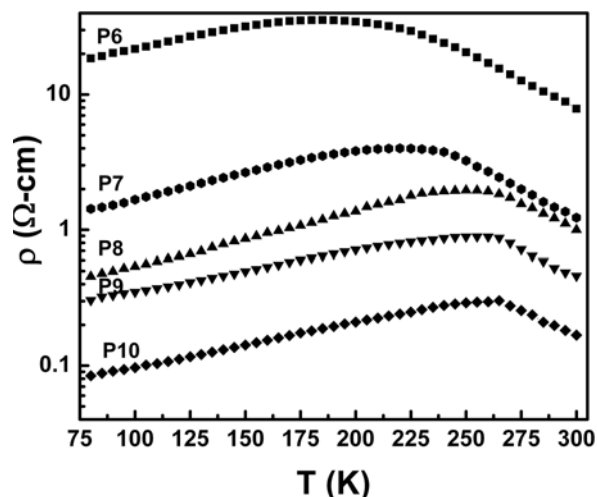


Fig. 5. Resistivity as a function of temperature at zero field of $\text{La}_{2/3}\text{Ca}_{1/3}\text{MnO}_3$ samples.

The resistivity of the samples increases as the sintering temperature decreases. The values of resistivity are 18.53Ω-cm, 1.43Ω-cm, 0.46Ω-cm, 0.31Ω-cm and 0.084Ω-cm at 80K while 7.84Ω-cm, 1.23Ω-cm, 0.99Ω-cm, 0.46Ω-cm and 0.17Ω-cm at room temperature (300K) for the samples P6, P7, P8, P9 and P10, respectively. Thus, the resistivity of sample P6 increases by more than two orders of magnitude as compared to sample P10. This increase in resistivity is caused due to enhanced scattering of the charge carriers by increasing the grain boundaries as particle size decreases by lowering the sintering temperature and due to presence of disorderness. On increasing the sintering temperature, the particle size increases leading to a decrease in grain boundaries and the associated disorder. This results in a decrease in scattering of the carriers expressed by a decrease in the resistivity. All the studied samples show an insulator ($d\rho/dT < 0$) to metal ($d\rho/dT > 0$) transition on lowering the temperature at a particular value (T_{IM}). The value of metal to insulator transition temperatures are $\sim 186\text{K}$, $\sim 225\text{K}$, $\sim 257\text{K}$, $\sim 261\text{K}$ and $\sim 272\text{K}$ for the samples P6, P7, P8, P9 and P10, respectively. Thus the value of transition temperature decreases (272K-186K) as the sintering temperature decreases from 1000°C to 600°C. The T_{IM} is an extrinsic property and strongly depends on the synthesis condition and microstructure (e.g. grain boundaries). The strong suppression in the value of T_{IM} with decreasing the sintering temperature is due to suppression of DE mechanism because of increase in non magnetic phase fraction, which is due to enhanced grain boundaries as a consequence of lower sintering temperature. Thus lowering the sintering temperature reduces the metallic transition temperature and increases the resistivity. It is

also noted that there is a large difference between the value of T_{IM} and T_c for smaller size particles sintered at lower temperatures. The variation of T_{IM} and T_c with sintering temperature is shown in Fig. 6. This difference is due to the fact that T_c is an intrinsic property and does not show the large change as a function of sintering temperature while T_{IM} is an extrinsic property that strongly depends upon the grain boundaries [24].

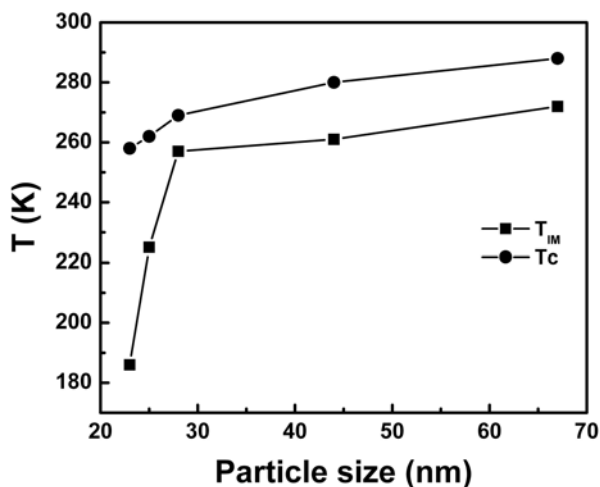


Fig. 6. Variation of insulator-metal transition temperature (T_{IM}) and PM-FM transition temperature (T_c) with sintering temperatures.

The magnetoresistance is the key property of these perovskite manganites. The temperature dependence of magnetoresistance (MR) in a field of 10 kOe for all the studied samples is shown in Fig. 7.

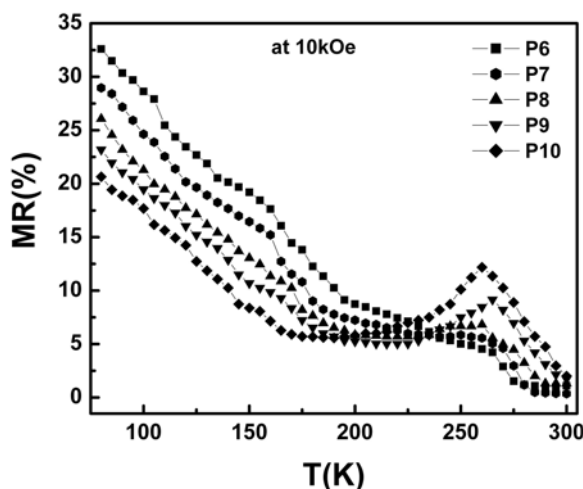


Fig. 7. Magnetoresistance (MR) as a function of temperature in a field of 10 kOe of $\text{La}_{2/3}\text{Ca}_{1/3}\text{MnO}_3$ samples.

The MR ratio is defined as $\text{MR} (\%) = [\rho(0, T) - \rho(H, T)] / \rho(H, T) \times 100\%$, where $\rho(0, T)$ and $\rho(H, T)$ are the resistivity values for zero and applied fields, respectively. All samples show the increase in MR at low temperature

($T < T_c$) as the sintering temperature decreases. The MR values at 80K are 32.6%, 28.9%, 26.1%, 23.2% and 20.6% for the samples P6, P7, P8, P9 and P10, respectively, at 10kOe. The maximum MR at 80K is observed for the sample P6 sintered at 600°C, i.e. the lowest sintering temperature. The appearance of peak in MR-T curve around T_c indicates the contribution of intrinsic component of MR, which arises due to DE mechanism around T_c . The peak MR values at 265K are 4.2%, 5.1%, 5.6%, 9.1% and 11.3% for the samples P6, P7, P8, P9 and P10, respectively. However, this peak around T_c is higher in the P10 sample sintered at 1000°C in comparison to other samples. The magnitude of MR peak around T_c decreases as we reduce the sintering temperature. Thus, lowering the sintering temperature leads to enhancement in low temperature MR ($T < T_c$) and reduction in MR in the high temperature region (around T_c) (see Table 2).

Table 2. Insulator-metal transition temperature (T_{IM}), Paramagnetic-ferromagnetic transition temperature (T_c) and magnetoresistance (MR) of the $\text{La}_{2/3}\text{Ca}_{1/3}\text{MnO}_3$ samples sintered at different temperatures.

Sintering temperature (°C)	T_{IM} (K)	T_c (K)	MR (%) at 10kOe	
			80K	265K
600	186	258	32.6	4.2
700	225	262	28.9	5.1
800	257	269	26.1	5.6
900	261	280	23.2	9.1
1000	272	288	20.6	11.3

In the manganites, two distinct contributions of MR have been pointed out so far. One is the intrinsic MR which arises due to suppression of spin fluctuations when the spins are all aligned in the sample on application of a magnetic field. This MR has the highest value near the ferromagnetic transition temperature and decreases as the temperature decreases. This is generally observed in the case of single crystal samples and single crystal thin films. In the polycrystalline samples, there is an additional MR, which is extrinsic in nature, arising due to the intergrain spin polarized tunneling across the grain boundaries present in the sample. This contribution usually increases as the temperature decreases. Until recently, it was believed that the former mechanism is responsible for the MR at high fields and the latter at low fields. But recent experiments have shown that the high-field response is also due to the existence of the grain boundary and the nature of grain boundary is a key ingredient in the mechanism of electric transport, since it constitutes the barriers through which carriers should cross or tunnel [4]. In our samples low field magnetoresistance (LFMR) at $T < T_c$ increases while high field magnetoresistance (HFMR) (around T_c) decreases with decreasing the sintering temperature. So, in present case, LFMR increases with decreasing the sintering temperature because we are increasing the disordered surface by decreasing the sintering temperature or particle size [18, 19]. The reduction in magnetization as the sintering temperature

decreases (Fig. 3) also supports the magnetic spin disorder induced by grain boundaries in the smaller particle samples and this spin disorder is suppressed by applying the magnetic field, resulting the enhancement in MR. The disappearance of HFMR (around T_c) in the smaller particle size samples can be explained by weakening of DE mechanism as sintering temperature is lowered. HFMR, which arises due to DE mechanism around T_c is mostly found in single crystal samples, so as we reduce the sintering temperature the DE mechanism is suppressed and HFMR decreases with decreasing the sintering temperature.

The magnetic field dependence of MR of all the studied samples measured in magnetic field range of 0-12 kOe at 80K is shown in Fig. 8.

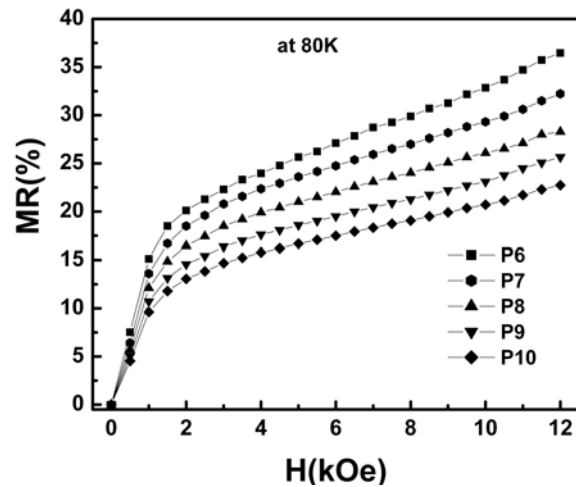


Fig. 8. Magnetoresistance (MR) as a function of magnetic field in the range (0-12 kOe) at 80K of $\text{La}_{2/3}\text{Ca}_{1/3}\text{MnO}_3$ samples.

Analysis of Fig. 8 shows that with increase in the magnetic field from 0 to 12 kOe, the MR of all the samples increases with increasing the magnetic field. The maximum MR is observed in sample P6 sintered at the lowest temperature (600°C). As the sintering temperature decreases, the MR increases. The value of MR at 80K for the sample P6 is 36.5% while it is 22.7% for the samples P10 at 12 kOe. It should also be noted that the variation of MR does not show any saturation in MR even up to 12kOe. This enhancement in MR as the sintering temperature decreases again caused through spin polarized tunneling at the grain boundaries.

4. Conclusions

We have successfully prepared the $\text{La}_{2/3}\text{Ca}_{1/3}\text{MnO}_3$ samples by sol-gel process and studied their magnetotransport properties with sintering temperature. All the samples have pure single LCMO perovskite phase with orthorhombic unit cells. Both T_{MI} and T_c shift towards lower temperature as the sintering temperature decreases. However the T_{MI} decreases substantially from

272K to 186K while T_c shows only slight decrease (288K-258K). It has been observed that LFMR ($T < T_c$) increases as the sintering temperature decreases but at the same time intrinsic MR (around T_c) decreases. This enhancement in LFMR for smaller size particles is due to enhanced spin polarized tunneling by increasing the grain boundary contribution as sintering temperature decreases.

Acknowledgments

The authors are grateful to Prof. O.N. Srivastava, Prof. D. Pandey (B.H.U.) and Dr. H.K. Singh (N.P.L.) for helpful discussions and encouragement. One of the authors (AG) is grateful to the University Grant Commission (UGC), New Delhi for the award of Senior Research Fellowship.

References

- [1] R. Von Helmolt, J. Wecker, B. Holzapfel, L. Schultz, K. Samwer, *Phys. Rev. Lett.* **71**, 2331 (1993).
- [2] S. Jin, T. H. Teifel, M. McCormack, R.A. Fastnacht, R. Ramesh, L. H. Chen, *Science* **264**, 413 (1994).
- [3] H. Y. Hwang, S. W. Cheong, P. G. Radaelli, M. Marezio, B. Batlogg, *Phys. Rev. Lett.* **75**, 914 (1994).
- [4] H. Y. Hwang, S. W. Cheong, N. P. Ong, B. Batlogg, *Phys. Rev. Lett.* **77**, 2041 (1996).
- [5] A. Gupta, G. Q. Gong, G. Xiao, P. R. Duncombe, P. Truilloud, P. Lecocur, Y. Y. Wang, V. P. Dravid, J. Z. Sun, *Phys. Rev. B* **54**, R15629 (1996).
- [6] R. Mahesh, R. Mahendiran, A. K. Raychaudhuri, C. N. R. Rao, *Appl. Phys. Lett.* **68**, 2291 (1996).
- [7] L. E. Hueso, J. Rivas, F. Rivadulla, M. A. Lopez-Quintela, *J. Appl. Phys.* **86**, 3881 (2000).
- [8] M. Ziese, *Rep. Prog. Phys.* **65**, 143 (2002).
- [9] X. L. Wang, S. X. Dou, H. K. Liu, M. Ionescu, B. Zeimet, *Appl. Phys. Lett.* **73**, 396 (1998).
- [10] C. Vazquez-Vazquez, M. C. Blanco, M. A. Lopez-Quintela, R. D. Sanchez, J. Rivas, S. Oseroff, *J. Mater. Chem.* **8**, 991 (1998).
- [11] C. J. Brinker, G. W. Scheres, *Sol-Gel Science*, Academic, New York, 1990.
- [12] P. N. Lisboa-Filho, A. W. Momburu, H. Pardo, W. A. Ortiz, E. R. Leite, *J. Phys. Chem. Solids* **64**, 583 (2003).
- [13] B. Vertruyen, A. Rulmont, R. Cloots, M. Ausloos, S. Dorbolo, P. Vanderbenden, *Mater. Lett.* **57**, 598 (2002).
- [14] L. W. Lei, Z. Y. Fu, J. Y. Zhang, *Mater. Lett.* **60**, 970 (2006).
- [15] K. S. Shankar, S. Kar, G. N. Subbanna, A. K. Raychaudhuri, *Solid State Commun.* **129**, 479 (2004).
- [16] Anurag Gaur, G. D. Varma, *J. Phys.: Condens. Matter* **18**, 8837 (2006).
- [17] H. Sun, Z.Y. Li, *Phys. Rev. B* **64**, 224413 (2001).
- [18] L. I. Balcells, J. Fontcuberta, B. Martinez, X. Obradors, *Phys. Rev. B* **58**, R14697 (1998).
- [19] T. Zhu, B. G. Shen, J. R. Sun, H. W. Zhao, W. S. Zhan, *Appl. Phys. Lett.* **78**, 3863 (2001).
- [20] Z. H. Wang, T. H. Ji, Y. Q. wang, X. Chen, R. W. Li, J. W. Cai, J. R. Sun, B. G. Shen, C. H. Yan, *J. Appl. Phys.* **87**, 5582 (2000).
- [21] H. De Keiysen Th, J. I. Langford, Mittemeijer, A. B. P. Vogels, *J. Appl. Cryst.* **15**, 308 (1982).
- [22] J. Rivas, L. E. Hueso, A. Fondado, F. Rivadullo, M. A. Lopez-Quintela, *J. Magn. Magn. Mater.* **21**, 57 (2000).
- [23] N. Zhang, W. Yang, W. Ding, D. Xing, Y. Du, *Solid State Commun.* **109**, 537 (1999).
- [24] A. de Andres, M. Garcia-Hernandez, J. L. Martinez, *Phys. Rev. B* **60**, 7328 (1999).

*Corresponding author: anuragdph@gmail.com